Variability of Tropical Cyclone Rapid Intensification in the North Atlantic and its Relationship with Climate Variations

Chunzai Wang[1], Xidong Wang[2], Robert H. Weisberg[3], and Michael L. Black[4]

[1]State Key Laboratory of Tropical Oceanography, South China Sea Institute of Oceanology, Chinese Academy of Sciences, Guangzhou, China

[2]College of Oceanography, Hohai University, Nanjing, China

[3]College of Marine Science, University of South Florida, St. Petersburg, FL USA

[4]NOAA-Atlantic Oceanographic and Meteorological Laboratory, Miami, FL USA

For publication in

Climate Dynamics

Abstract

The paper uses observational data from 1950 to 2014 to investigate rapid intensification (RI) variability of tropical cyclones (TCs) in the North Atlantic and its relationships with large-scale climate variations. RI is defined as a TC intensity increase of at least 15.4 m/s (30 knots) in 24 h. The seasonal RI distribution follows the seasonal TC distribution, with the highest number in September. Although an RI event can occur anywhere over the tropical North Atlantic (TNA), there are three regions of maximum RI occurrence: (1) the western TNA of 12°N–18°N and 60°W–45°W, (2) the Gulf of Mexico and the western Caribbean Sea, and (3) the open ocean southeast and east of Florida. RI events also show a minimum value in the eastern Caribbean Sea north of South America—a place called a hurricane graveyard due to atmospheric divergence and subsidence. On longer time scales, RI displays both interannual and multidecadal variability, but RI does not show a long-term trend due to global warming. The top three climate indices showing high correlations with RI are the June-November ENSO and Atlantic warm pool indices, and the January-March North Atlantic oscillation index. It is found that variabilities of vertical wind shear and TC heat potential are important for TC RI in the hurricane main development region, whereas relative humidity at 500 hPa is the main factor responsible for TC RI in the eastern TNA. However, the large-scale oceanic and atmospheric variables analyzed in this study do not show an important role in TC RI in the Gulf of Mexico and the open ocean southeast and east of Florida. This suggests that other factors such as small-scale changes of oceanic and atmospheric variables or TC internal processes may be responsible for TC RI in these two regions. Additionally, the analyses indicate that large-scale atmospheric and oceanic variables are not critical to TC genesis and formation; however, once a tropical depression forms, large-scale climate variations play a role in TC intensification.

1. Introduction

An improvement in the forecasting and understanding of tropical cyclones (TCs) is very important because it can help reduce loss and damage caused by TCs. The causes of TC track and intensity changes are two issues that have been focused on by the scientific community during the past decades. Significant improvements have been made in the forecasting of TC tracks over the past decades (Rappaport et al. 2009; Elsberry 2014). However, the forecasting of TC intensity change has not improved as rapidly, especially the forecasting of TC rapid intensification (RI) (e.g., Elsberry et al. 2007; Rappaport et al. 2009; Chen et al. 2011; Elsberry 2014). RI is usually defined as a maximum sustained surface wind speed increase of at least 15.4 m/s (30 knots) over a 24-h period. The relatively low skill of intensity forecasts is primarily due to the complexity of TC RI processes, which involves small- and large-scale changes, TC internal processes, and multi-scale interactions between TCs and the atmospheric and oceanic environment. There is no doubt that a hurricane undergoing an unanticipated RI immediately prior to landfall will generate very large losses. Therefore, the accurate forecasting of TC RI is very important from societal and economic as well as scientific points of view. A better understanding of RI will help improve the forecasting of TC intensity. Lee et al. (2016) recently found a bimodality of the global TC lifetime maximum intensity distribution, emphasizing that RI plays an important role in the TC climatology.

Many studies have focused on TC intensification; however, fewer studies have examined TC RI. In the North Atlantic, Kaplan and DeMaria (2003) and Kaplan et al. (2010) showed large-scale atmospheric and oceanic characteristics associated with TC RI. Klotzbach (2012) attempted to show potential impacts of interannual tropical Pacific ENSO events and intraseasonal variations of the Madden-Julian oscillation on TC RI in the North Atlantic basin.

However, the long-term variation of TC RI in the North Atlantic and its detailed relationships with climate phenomena and large-scale oceanic and atmospheric variables are largely unknown. We do not know whether the large-scale environment modulates the RI frequency and location on longer time scales. The purpose of the present paper is to document and address these issues.

The paper is organized as follows. Section 2 introduces the data sets and methods used in this study. Section 3 briefly summarizes and examines seasonal and spatial distributions of RI events in the North Atlantic basin. Section 4 shows the variability of RI in the North Atlantic and its relationships with climate indices. In Section 5, we examine large-scale environmental variables related to RI variations. We then show contributions of climate phenomena to large-scale environmental variables responsible for TC RI in Section 6. Finally, we give a summary and discussion.

2. Data and Methods

The TC data set is from the HURDAT2 database archived by the International Best Track Archive for Climate Stewardship (IBTrACS) from 1950 to 2014 in the North Atlantic, which consists of the 6-hour estimates of position, maximum sustained surface wind speed and central pressure. This TC data set is used to identify the occurrence of RI. Following Kaplan and DeMaria (2003) and Kaplan et al. (2010), we define an RI event as an intensity increase of at least 15.4 m/s (30 knots) over a 24-h period. This is equivalent to the 95th percentile of over-water 24-h intensity changes of Atlantic basin TCs (Kaplan and DeMaria 2003; Kaplan et al. 2010, 2015).

The Saffir-Simpson hurricane scale is a classification used for all TCs that include tropical depressions, tropical storms and hurricanes. TCs with maximum surface winds of 10–17 m/s (20–33 knots) are classified as tropical depressions. If a tropical depression reaches winds

of at least 18 m/s (34 knots), it receives a name and is classified as a tropical storm (TS). If a TS continues to intensify and reaches maximum sustained winds of 33 m/s (64 knots), then the TS is designated as a hurricane (H). Hurricanes are further classified into Category 1–5 hurricanes which have maximum sustained winds of 33–42 m/s (64–82 knots), 43–49 m/s (83–95 knots), 50–58 m/s (96–112 knots), 59–69 m/s (113–136 knots), and at least 70 m/s (137 knots), respectively. Major hurricanes (MH) are defined to include Category 3–5 hurricanes.

Oceanic variables, which can determine TC intensity, include sea surface temperature (SST) (e.g., Emanuel et al. 2004) and tropical cyclone heat potential (TCHP) (e.g., Shay et al. 2000; Lin et al. 2005, 2008, 2009a, 2009b). The monthly data set of the extended reconstructed SST version 3 is used and obtained from the NOAA National Climatic Data Center, with a horizontal resolution of 2° × 2° (Smith et al. 2008). TCHP represents ocean heat content contained in the waters warmer than 26 °C (e.g., Leipper 1967; Leipper and Volgenau 1972):

$$TCHP = c_p \int_{D_{26}}^{0} \rho(z)[T(z) - 26]\, dz,$$

where c_p is specific heat at constant pressure (3.9 kJ/kg K), D_{26} is the depth of the 26 °C isotherm, $\rho(z)$ is the in-situ density, and $T(z)$ is the in-situ temperature. TCHP is calculated by using the monthly mean temperature-salinity data from the Simple Ocean Data Assimilation (SODA) with a horizontal resolution of 0.5° × 0.5° and 40 vertical levels (Carton and Giese 2008). The calculation of TCHP in this paper is from 1950 to 2010 because of SODA availability, but all of the other variables and analyses are from 1950 to 2014.

Large-scale atmospheric environmental factors such as vertical wind shear (VWS) between 200 and 850 hPa (e.g., Merrill 1988; Kaplan and DeMaria 2003) and relative humidity (RHUM) at 500 hPa (Shu et al. 2012) also play a role in the RI process. VWS and RHUM are

obtained from the National Centers for Environmental Prediction-National Center for Atmospheric Research (NCEP-NCAR) reanalysis fields (Kalnay et al. 1996). As in other studies, VWS is calculated as the magnitude of the vector difference between winds at 200 and 850 hPa. We also used the Twentieth Century Reanalysis version 2 (Compo et al. 2011) and obtained similar results (not shown).

Climate indices used in this study include the NINO3.4 SST anomalies in the region of 5°S–5°N, 170°W–120°W, the Atlantic multidecadal oscillation (AMO) index, the North Atlantic oscillation (NAO) index, the SST anomalies in the hurricane main development region (MDR) [The MDR is defined as the region from 10°N–20°N, 85°W–15°W which is similar to that by Goldenberg and Shapiro (1996)], and the Atlantic warm pool (AWP) index. The AMO index is calculated as the detrended SST anomalies of the North Atlantic from the equator to 70°N (Enfield et al. 2001). The AWP index is calculated as the anomaly of the area of SST warmer than 28.5 °C divided by the climatological mean AWP area (Wang et al. 2008), which is comprised of the Gulf of Mexico, the Caribbean Sea and the western tropical North Atlantic (TNA). The NAO index is defined as the principal component time series of the first leading mode of rotated empirical orthogonal function analysis of monthly mean 500-mb height over the Northern Hemisphere. All of these climate indices are calculated during the Atlantic hurricane season of June to November (JJASON), except for the NAO index which is also computed during the winter months of January to March (JFM). All of these climate indices are linearly detrended and standardized.

The simple methods of linear correlation and linear regression are used in this study. For the significance test, we calculate the effective degrees of freedom (e.g., Quenouille 1952; Medhaug and Furevik 2011; Wang et al. 2012) as: $NE = N/(1 + 2R_{X1}R_{Y1} + 2_{RX}2R_{Y2})$, where N is

the number of data points for the time series of X and Y; R_{X1} or R_{Y1} is the autocorrelation at lag one; and R_{X2} or R_{Y2} is the autocorrelation at lag two. For some cases, we separate a variation into interannual and decadal-multidecadal variability. The decadal-multidecadal variability is obtained by performing a 7-year low-pass filter to the detrended oceanic and atmospheric variables. The interannual variability is calculated by subtracting the decadal-multidecadal variability from the detrended time series.

3. Seasonal and Spatial Distributions of RI Events

Before we examine the longer term variations of RI events in the North Atlantic, we first briefly summarize and examine the seasonal and spatial distributions of RI events. Figure 1 compares the seasonal distribution of the RI number with that of the TC number in the North Atlantic, and shows the percentage of TCs undergoing RI. Not surprisingly, the seasonal RI distribution follows the seasonal TC distribution, with the highest number in September. This is because more TC genesis events increase the probability for RI occurrence. This also suggests that the seasonal cycle of large-scale oceanic and atmospheric variables may have a similar effect on RI occurrence with that on formation and development of TCs in the North Atlantic basin. In addition to the highest percentage of TCs undergoing RI in September, the RI ratio shows a higher value in November (Fig. 1c). The relatively higher RI ratio in November than in October is due to that few TCs form in the late season of November, but the RI number in November is not relatively small. During the TC late season, most of TCs form in the Gulf of Mexico and Caribbean Sea. As will be shown later, the Gulf of Mexico and western Caribbean Sea is a region where RI is relatively easy to occur. However, large-scale oceanic and atmospheric variables may not be responsible for TC RI in this region. Other factors such as ocean warm eddies may intensify TCs in the Gulf of Mexico (Shay et al. 2000; Hong et al. 2000).

The spatial distributions of oceanic and atmospheric variables of SST, TCHP, VWS and RHUM in September are shown in Fig. 2. The SST is high in the entire TNA, with the highest values in the Atlantic warm pool (AWP) region of the Gulf of Mexico, the Caribbean Sea and the western TNA because the AWP is peaked in September (Wang and Enfield 2001). The largest values (above 60 kJ/cm^2) of TCHP are near the Caribbean Sea. Low VWS is located in the TNA between 10°N and 15°N. For RHUM, a band of high humidity extends from West Africa to the eastern TNA. All of these favorable conditions contribute to the seasonal peak of Atlantic TC activity in September.

The 24-h tracks of RI events are shown in Fig. 3a and the spatial distribution of the RI number in each 5° × 5° grid box is shown in Fig. 3b. During 1950–2014, the North Atlantic had a total of 988 TCs (including tropical depressions). Of these 988 TCs, 215 TCs experienced at least one time of RI. Although an RI event can occur almost anywhere over the TNA, three regions of maximum RI occurrence are in (1) the western TNA from approximately 12°N–18°N and 60°W–45°W, (2) the Gulf of Mexico and western Caribbean Sea, and (3) the open ocean southeast and east of Florida. RI events also show a minimum value in the eastern Caribbean Sea north of South America. The RI minimum in the eastern Caribbean Sea is consistent with the climatology there which features local lower-tropospheric divergence and subsidence (Shieh and Colucci 2010) in association with the Caribbean low-level jet (CLLJ) (Wang 2007). Wang (2007) showed that the strong easterly CLLJ at 925 hPa results in the lower-tropospheric divergence east of the CLLJ core because of the acceleration of winds upstream of the CLLJ. Wang (2007) also suggested that the easterly CLLJ increases the moisture flux divergence in the Caribbean and thus suppresses the convection, decreasing rainfall and suppressing TC activity. These are consistent with the results of Shieh and Colucci (2010) who showed that lower-

tropospheric divergence and subsidence are unfavorable for TC genesis and development. For years, hurricane forecasters have called the eastern Caribbean Sea a hurricane graveyard. The minimum of RI events in the eastern Caribbean shown in Fig. 3b supports these previous results.

4. Variability of RI and Climate Indices

The time series of the annual RI number from 1950 to 2014 is shown in Fig. 4. The RI time series does not show an obvious trend from 1950 to 2014, suggesting that the variation of RI in the North Atlantic does not yet show a trend due to global warming. However, the RI time series displays both interannual and decadal-multidecadal variability. The decadal-multidecadal variability resembles the AMO variation, with low values of RI during the 1980s and early 1990s and high values of RI before the 1980s and after the middle 1990s. Because of the RI multidecadal feature, we hereafter refer to this variation as multidecadal variability.

To quantify the relationships of RI with climate indices, we calculate the correlations between the RI time series and climate indices of ENSO, the NAO, the AMO, MDR SST, and the AWP (Table 1). RI is significantly (above the 95% significance level) correlated with the June-November (JJASON) ENSO, MDR SST and AWP indices, but insignificantly correlated with the JJASON AMO and NAO indices. The insignificant correlation with the JJASON AMO is not surprising since the center of maximum SST anomalies associated with the AMO is in the high latitudes rather than in the tropics (e.g., Enfield et al. 2001). With regards to the NAO, RI is significantly and negatively related to the January-March (JFM) NAO index. This is because the mid-latitude atmosphere is most energetic during the winter NAO (Hurrel 1996). Thus, the winter NAO anomalies are more likely a better representation of the mid-latitude atmosphere than the summer and fall anomalies. The NAO linkage may be through the processes that the zonal wind forcing associated with a negative (positive) phase of the NAO results in weaker

(stronger) trade winds which induce a warming (cooling) subtropical and tropical Atlantic Ocean (e.g., Enfield et al. 2006).

During the winter months, when intrinsic mid-latitude atmospheric variability is most energetic, the atmosphere imparts an SST "footprint" onto the ocean via changes in the surface heat flux (Vimont et al. 2001). Vimont et al. (2003) further pointed out that the general feature of the footprint mechanism is not necessarily confined to the North Pacific. In fact, a similar mechanism also exists in the Atlantic. Using a simple and theoretical coupled ocean–atmosphere model, Xie (1999) showed that extratropical anomalies in the North Atlantic can extend into the tropics and provide the forcing for the tropics, under which the wind-evaporation-SST feedback acts to produce tropical variability. Physically, the NAO in the winter induces an SST change through the heat flux change and then the NAO-induced SST anomalies are maintained and developed by local positive feedback processes to the summer and fall. The local positive ocean–atmosphere feedbacks can be the wind-evaporation-SST feedback proposed by Xie and Philander (1994) and/or the longwave radiation feedback associated with cloudiness by Wang and Enfield (2003). During the summer and fall, the SST footprint in the tropics forces atmospheric circulation anomalies that in turn affect TC RI during the Atlantic hurricane season of JJASON.

Table 1 shows that the top three climate indices with high RI correlations are the JJASON NINO 3.4 and AWP indices, and the JFM NAO index. Thus, we examine and compare these three climate indices with the RI time series (Figs. 5, 6, 7). To better compare the RI time series with the climate indices, we standardize the RI time series and superimpose it on the climate indices. Multidecadal variability is obtained by performing a 7-year low-pass filter to the total index, and interannual variability is calculated by subtracting the multidecadal variability

from the total index. The total NINO3.4 and NAO indices are negatively related to the RI time series, whereas the total AWP index is positively associated with the RI number. These indicate that the positive phases of ENSO and the NAO are unfavorable for RI of TCs, whereas the local ocean temperature increase in the TNA tends to rapidly intensify Atlantic TCs.

On interannual time scales, it seems from Figs. 5b, 6b and 7b that all climate indices except for NINO3.4 are not highly related to the RI time series. Indeed, the correlation calculations in Table 2 do show that the NINO3.4 SST anomaly index is the only one that shows a significant (above the 95% confidence level) correlation with the RI time series on interannual time scales. This indicates that ENSO is a dominant climate factor for controlling RI of TCs on interannual time scales due to ENSO's impacts on Atlantic basin vertical wind shear (e.g., Gray 1984; Goldenberg and Shapiro 1996). A La Niña condition in the tropical Pacific is favorable for a TC to rapidly intensify in the Atlantic, whereas an El Niño is unfavorable.

On multidecadal time scales, Figs. 5c, 6c and 7c seem to show that the indices of the AWP and NAO indices are highly related to the RI time series, but the NINO3.4 index is not. The correlations in Table 3 indeed show that all climate indices except ENSO and the AMO are significantly (above the 95% confidence level) correlated with the RI time series on multidecadal time scales. It seems surprising that the AMO does not significantly correlate with RI on multidecadal time scales. However, this may be understandable given that the center of maximum SST anomalies of the AMO is in the high latitudes rather than in the tropics (Delworth and Mann 2000; Enfield et al. 2001) and the effect of the AMO on TC activity operates via the AWP-induced atmospheric changes (Wang et al. 2008). Table 3 also shows that the highest RI correlation is the AWP index, which is consistent with the previous study of Wang et al. (2008)

that the AWP acts as a link between climate and Atlantic TC activity on multidecadal time scales.

In the last section, we showed that the seasonal RI distribution follows the seasonal TC distribution, with the peak of RI events in September. Are the variations of RI on longer time scales similar to those of the TC number in the North Atlantic? To answer this question, we plot the numbers of TC, TS, H and MH in Fig. 8. The variations of these numbers, to some degrees, are similar to those of RI events (Figs. 5. 8). However, a close examination reveals that the similarity is mostly on interannual time scales. The correlation calculations in Table 4 show that RI is significantly (above the 95% significance level) correlated with the numbers of TC, TS, H and MH on interannual time scales. On multidecadal time scales, RI is significantly correlated with the numbers of TS, H and MH. In fact, the time series of TS, H and MH do show a clear multidacadal variation like RI, whereas the TC time series does not display a multidecadal variation (Figs. 4, 8). In particular, the phase of the MH number clearly resembles the multidecadal variation of RI events because most MHs undergo RI during their lifetime (the percentage of MHs that undergo RI is 70%).

To see the climate impact differences between the TC numbers and RI events, we also calculate the correlations of climate indices with the numbers of TC, TS, H and MH (Tables 1, 2, 3). Unlike the RI case, the total number of TCs is not significantly correlated with any climate indices as shown in Table 1. However, when a tropical depression intensifies to reach the intensity of TS, H or MH, correlations with climate indices start to be statistically significant. This suggests that the genesis and formation of tropical depressions do not seem to highly relate to large-scale climate phenomena. However, once a tropical depression forms, favorable conditions of large-scale climate variations can make the tropical depression intensify and/or

rapidly intensify. In other words, although large-scale climate variations can provide favorable environmental conditions for TCs to intensify or rapidly intensify, individual cyclogenesis events are probably triggered by small-scale disturbances such as synoptic-scale perturbations of African easterly waves. Physically, tropical depressions can form in marginal environments, whereas TS, H, MH and RI need more favorable environments. This may explain why the total number of TCs in the North Atlantic does not show a multidecadal variation associated with the AMO, but the numbers of TS, H, MH and RI do.

5. Large-Scale Environmental Factors related to RI

In this section, we attempt to examine the spatial distributions of possible environmental factors responsible for the RI variations. In order for a TC to rapidly intensify, several oceanic and atmospheric conditions likely need to be satisfied. SSTs need to be very warm. Water temperatures need to be sufficiently warm through a relatively large depth of the ocean, which is represented and measured by TCHP. Atmospheric vertical wind shear needs to be low. When wind shear is high, the convection and circulation of the cyclone will be disrupted (e.g., Gray 1979; Kaplan and DeMaria 2003; Shu et al. 2012). Additionally, high relative humidity values in the mid-troposphere are necessary for TC development (e.g., Gray 1979, 1988). Thus, here we focus on the spatial distributions of large-scale oceanic and atmospheric variables such as SST, TCHP, VWS and RHUM associated with RI (Fig. 9). In these regression calculations, we do not separate them into interannual and multidecadal variations because the interannual and multidecadal regressed patterns are similar to the total regressions shown in Fig. 9.

The SST regressed patterns show a significant (above the 95% significance level) positive regression in the eastern Caribbean Sea just north of South America. However, this region shows a minimum of RI events (Fig. 3), suggesting that the SST in the TNA may not be a

major factor for the RI variations. TCHP of the upper layer ocean shows a positive regression in the Caribbean Sea and the western TNA. The negative VWS regression values cover almost the entire MDR. These suggest that TCHP and VWS are important for TC RI in the MDR. The regressed pattern of 500-hPa RHUM displays a significant positive regression east of 50°W in the TNA. This indicates that if a TC forms in the eastern TNA, RHUM is a factor responsible for the TC to rapidly intensify.

The climatological mean RI number in Fig. 3 shows that the Gulf of Mexico and the open ocean southeast and east of Florida are also important regions for TCs to rapidly intensify, in addition to the western MDR. However, none of the large-scale oceanic and atmospheric variables analyzed here are significantly responsible for TC RI in these two regions. This suggests that other factors such as small-scale changes of oceanic and atmospheric variables or TC internal processes may be responsible for a TC to rapidly intensify in the Gulf of Mexico and the open ocean southeast and east of Florida. In fact, Shay et al. (2000) used observational data to examine the impact of a Gulf of Mexico eddy on the intensity of Hurricane Opal, and concluded that the ocean warm eddy may have contributed to Opal's RI. The numerical modeling results of Hong et al. (2000) also supported the importance of the Gulf of Mexico eddy in a hurricane's intensification.

We also examine the spatial distributions of SST, TCHP, VWS and RHUM associated with the numbers of TC, TS, H and MH. Figure 10 shows regressions of the TC number onto the SST, TCHP, VWS and RHUM during JJASON. The number of TCs does not show a significant relationship with these large-scale oceanic and atmospheric variables. However, when a tropical depression is further developed, the large-scale oceanic and atmospheric variables become more and more important. In particular, when a TC reaches a strength above the intensity of a

hurricane, the distribution patterns of SST, TCHP, VWS and RHUM are similar to those associated with RI events (Fig. 11 versus Fig. 9). This is not a surprising result since about 52% of hurricanes experienced at least one time of RI in the North Atlantic. Additionally, we also perform the analyses of environmental composite differences between active and inactive years of TC, TS, H and MH (not shown). We find that SST difference in the MDR is not statistically significant for the TC case, whereas the SST differences are significant for those of TS, H and MH. The composite results are similar to those in Figs. 10 and 11. This further supports the argument that the large-scale environment is not critical to TC genesis and formation, but it is important to TC intensification.

The above regression analyses show that the variations of TCHP, VWS and RHUM are important for TC RI in the MDR region. The time series of TCHP, VWS and RHUM in the MDR during JJASON are shown in Fig. 12 and their correlations with RI, TC, TS, H and MH are displayed in Table 5. Statistically, TCHP, VWS and RHUM in the MDR are significantly correlated with RI. The time series of VWS shows both interannual and multidecadal variations, whereas those of TCHP and RHUM vary mainly on interannual time scales without an obvious multidecadal signal. A comparison of Fig. 12b with Fig. 4 shows that the RI multidecadal variation is consistent with that of VWS, suggesting that the large-scale VWS multidecadal variation plays an important role in the RI multidecadal variation. However, TCHP and RHUM are significantly related to RI mainly on interannual time scales. Again, Table 5 shows that the numbers of TC are not correlated with TCHP, VWS and RHUM. However, when a tropical depression reaches at least TS intensity, the correlations with TCHP, VWS and RHUM start to become significant.

6. Influences of Climate Phenomena on Large-Scale Environmental Factors

The last section has shown the spatial patterns of large-scale environmental variables of SST, TCHP, VWS and RHUM associated with RI variations in the North Atlantic. In this section, we examine and show what causes the variations of SST, TCHP, VWS and RHUM, i.e., the contributions of climate phenomena to these large-scale oceanic and atmospheric variables.

Table 1 shows that the top three climate indices of high correlations with RI are the JJASON NINO3.4 and AWP indices, and the JFM NAO index. The question is: Are these three climate phenomena attributable to the variations of SST, TCHP, VWS and RHUM? We first examine the regressions of NINO3.4 index onto SST, TCHP, VWS and RHUM during JJASON (Fig. 13). Significant (above the 95% significance level) correlations between ENSO and VWS exist in the MDR and Caribbean Sea. This is consistent with previous studies that ENSO affects Atlantic TC activity through the change of VWS (e.g., Gray 1984; Goldenberg et al. 2001; Vecchi and Soden 2007). On the other hand, the AWP can significantly affect variations of SST, TCHP, VWS and RHUM in the TNA (Fig. 14). A comparison of Fig. 14 with Fig. 9 shows that AWP-related changes of SST, TCHP, VWS and RHUM can explain those associated with the RI variation. The significant influences of the wintertime NAO are on the SST and TCHP changes in the western MDR (Fig. 15a, 15b). Figure 15c shows that the NAO positively increases VWS in the TNA between 10°N–20°N, but the influence is not statistically significant. As shown in Fig. 15d, the NAO can significantly reduce RHUM in the western portion of the MDR.

We also calculate the regressions of the JJASON AMO and MDR SST anomalies and JJASON NAO index onto SST, TCHP, VWS and RHUM during JJASON (not shown). As expected, the regressed patterns for the AMO and MDR SST anomalies are similar to those for the AWP index in Fig. 14. This is because when the AMO is in its warm (cold) phase, the AWP

is large (small) (Wang et al. 2006, 2008) although the largest SST anomalies of the AMO are located in the high latitudes of the North Atlantic. The same is true for the MDR SST anomalies. The regressed patterns for the JJASON NAO index are also similar to those for the JFM NAO index in Fig. 15, except for RHUM. The JJASON NAO index does not show a significant RHUM regression in the MDR.

These regression calculations seem to suggest that the AWP variations can explain or account for most of the SST, TCHP, VWS and RHUM changes associated with the RI variations. However, we must keep in mind that climate phenomena are not independent. In other words, the AWP variations are indirectly related to other climate variations (e.g., Wang et al. 2006; Enfield et al. 2006; Zhang and Wang 2012). For example, Zhang and Wang (2012) identified 17 large AWPs from 1950 to 2010 when the AWP index is larger than at least 25% for three consecutive months from June to November. Of the 17 large AWPs, ten large AWPs in the summer and fall are preceded by an El Niño event in the tropical Pacific during the preceding winter, whereas seven large AWPs are not preceded by an El Niño event in the preceding winter. These seven large AWP years except 2008 are associated with the negative phase of the NAO in the simultaneous summer or fall. It seems that a combination of ENSO and the NAO can explain the AWP variations. Both ENSO and the NAO can remotely influence the SST anomalies in the TNA which then affect oceanic and atmospheric variables by local processes and local ocean–atmosphere coupling.

7 Summary and Discussion

As stated in the Introduction, significant improvement has been made in the forecasting of TC tracks during the past decades. However, the forecasting of TC intensity change has not been improved much, especially for the forecasting of TC rapid intensification (RI) defined as a

TC intensity increase of at least 15.4 m/s (30 knots) in 24 h. This is due to our poor understanding and simulation of RI processes associated with various temporal and spatial scales. The present paper focuses on the impacts of large-scale climate factors on TC RI in the North Atlantic basin by analyzing available observational data from 1950 to 2014. In the North Atlantic, the seasonal RI distribution follows the seasonal TC variation with the highest number in September since more TC genesis increases the probability of RI occurrence. It is also shown that although an RI event can occur almost anywhere over the tropical North Atlantic (TNA), there are three regions of maximum RI occurrence: (1) the western TNA in the region of 12°N–18°N and 60°W–45°W, (2) the Gulf of Mexico and the western Caribbean Sea, and (3) the open ocean southeast and east of Florida. We also find an RI minimum region in the eastern Caribbean Sea north of South America, consistent with the previous studies by Wang (2007) and Shieh and Colucci (2010) who showed local lower-tropospheric divergence and subsidence in association with the Caribbean low-level jet. The RI minimum region supports that the eastern Caribbean Sea is a hurricane graveyard.

The time series of the annual RI number shows both interannual and multidecadal variability, but it does not display a long-term trend. The lack of the long-term trend suggests that global warming may not contribute to TC RI in the North Atlantic. On interannual time scales, the RI variation is significantly correlated with the numbers of TCs, tropical storms, hurricanes and major hurricanes. However, on multidecadal time scales, RI is significantly correlated with the numbers of tropical storms, hurricanes and major hurricanes. This is because the number of tropical depressions in the North Atlantic basin does not show a multidecadal variation. The RI multidecadal variability resembles the AMO variation, with low values of RI during the 1980s and early 1990s and high values of RI before the 1980s and after the middle

1990s. The RI multidecadal variability is consistent with the VWS multidecadal variation in the Atlantic hurricane MDR.

The top three climate indices, which show high correlations with RI, are the JJASON ENSO and AWP indices, and the JFM NAO index. The ENSO impact is mainly on interannual time scales because of the dominant effect of the interannual ENSO climate phenomenon, whereas the others are on multidecadal time scales. It seems surprising that the AMO is not significantly correlated with RI on any time scales. This may be explained from the following points of view. First, although the AMO represents a basin-wide SST variation in the North Atlantic, its center of maximum SST anomalies is in the high latitudes rather than in the tropics (e.g., Delworth and Mann 2000; Enfield et al. 2001). Second, the periods for large and small AWPs coincide with the warm and cool phases of the AMO (Wang et al. 2008). As a result, the influences of the AMO on TC activity and climate may operate through the atmospheric changes induced by the AWP. Third, the AWP is in the path of or the birthplace of TCs in the Atlantic basin. Fourth, warm pool size (SST $\geq$28.5 °C) is an expression of SST anomalies, but is an index weighted toward regions of maximum SST where deep convective heating occurs. Therefore, the impacts of the ocean temperatures on RI multidecadal variability do not necessarily need a high correlation with the AMO index as long as the atmospheric convective condition is satisfied and conditions induced by tropical ocean temperature changes are favorable for a TC to rapidly intensify.

The NAO represents a mid- or high-latitude atmospheric variation in the North Atlantic. The mid-latitude atmosphere of the NAO is most energetic in the winter and relatively quiet in the summer (e.g., Hurrel 1996), so the winter anomalies are more likely a better representation of mid-latitude atmospheric variability than the annually averaged anomalies. The winter NAO

variation in the mid-latitudes influences tropical variability during the following summer and fall via the footprint mechanism (e.g., Vimont et al. 2001, 2003) or the extension of extratropical anomalies maintained by ocean–atmosphere interactions in the tropics (Xie 1999). During the winter months of energetic mid-latitude atmospheric variability, the atmosphere imparts an SST footprint onto the ocean via change in the surface heat flux. The SST footprint persists into the summer and fall seasons, when the mid-latitude atmosphere is more quiescent. The SST footprint forces an atmospheric circulation anomaly in the subtropical and tropical regions. This explains why the JFM NAO index is highly related to RI, but the JJASON NAO index is not.

The western TNA is one of three regions of maximum RI occurrence in the North Atlantic basin. Our regression calculations show that in this region RI is significantly related to TCHP of the upper layer ocean and atmospheric VWS, indicating that high TCHP and low VWS are favorable for RI occurrence there. The regressed pattern of 500-hPa RHUM displays a significant positive regression east of 50°W in the TNA. This suggests that if a TC forms in the eastern TNA, RHUM may be a factor responsible for the TC to rapidly intensify.

For the other two maximum RI regions in the Gulf of Mexico and the western Caribbean Sea and in the open ocean southeast and east of Florida, we find that none of the large-scale oceanic and atmospheric variables are responsible for TC RI. This suggests that other factors and processes may be attributable to TC RI in these two regions. Previous studies have shown that upwelling and vertical mixing of the cool underlying ocean by the TC vortex can produce a negative feedback between the atmosphere and ocean (e.g., Sutyrin and Khain 1984; Bender and Ginis 2000). However, Shay et al. (2000) and Hong et al. (2000) suggest that ocean warm eddies may reduce the magnitude of the mixing of subsurface water, thereby decreasing the magnitude of this negative feedback and thus increasing TC intensity in the Gulf of Mexico. Another

example is the effect of ocean salinity. The upper ocean salinity distribution largely affects the stratification and stability which in turn influence the vertical mixing of the upper layer ocean and upwelling of cooler subsurface ocean water. A recent study by Balaguru et al. (2012) shows that the salinity-induced barrier layer can intensify a TC, suggesting the importance of salinity in TC activity. It seems to be obvious that salinity variability will change the energy of a TC supplied by the underlying ocean.

We also compare the spatial distributions of large-scale environmental factors associated with the numbers of RI, TCs, tropical storms, hurricanes and major hurricanes. Our analyses show that the number of TCs does not show a significant relationship with these large-scale oceanic and atmospheric variables. However, when a tropical depression is further developed above TS intensity, large-scale oceanic and atmospheric variables become more and more important. In particular, when a TC reaches hurricane strength, the distribution patterns of SST, TCHP, VWS and RHUM are similar to those associated with RI. This is not a surprising result since about 52% of hurricanes experienced at least one time of RI in the North Atlantic. The analyses suggest that large-scale atmospheric and oceanic variables are not critical to TC formation which requires a pre-existing near-surface organized disturbance with sufficient vorticity and convergence. The pre-existing organized disturbance does not necessarily relate to large-scale atmospheric and oceanic variations. However, once a tropical depression forms, large-scale climate variations start to influence it and play a role in its intensification or RI. This also explains why the total TC number in the North Atlantic do not vary greatly with the AMO, but intense hurricanes show a strong variation with the AMO.

We discuss the contributions of climate phenomena to large-scale oceanic and atmospheric variables related to RI. Among all of the climate phenomena examined here, ENSO,

the AWP and the NAO are the top three climate variations whose indices show high correlations with RI. ENSO's impact is on atmospheric VWS, whereas the significant influences of the NAO are on oceanic SST and TCHP changes. On the other hand, the AWP can explain or account for most of the SST, TCHP, VWS and RHUM changes associated with the RI variation. However, we must keep in mind that climate phenomena are not independent. Other climate phenomena can influence the SST anomalies in the TNA which then affect oceanic and atmospheric variables related to RI.

Hendricks et al. (2010) examined environmental control on TC intensity changes in both the western North Pacific and North Atlantic. They concluded that the rate of intensification is not largely dependent on the environmental conditions. However, some of their results in the North Atlantic basin are not inconsistent with our analyses presented in the present paper. For example, their Fig. 5 shows that in the North Atlantic basin rapidly intensifying events occurred in environment with weaker vertical wind shear than other regular-intensifying events, which is consistent with our result that low VWS is favorable for RI occurrence in the hurricane MDR.

Our analyses in this paper are through linear correlations and regressions. It is thus important to discuss nonlinearities between hurricane occurrence and large scale climate variables. Emanuel and Nolan (2004) proposed an empirical index of the Genesis Potential Index (GPI) for considering the influence of atmospheric and oceanic variables on TC genesis. The GPI nonlinearly depends on the four large-scale environmental factors of the absolute vorticity at 850 hPa, relative humidity at 700 hPa, potential intensity, and vertical wind shear between 200 and 850 hPa. Recently, Jiang et al. (2012) linearized this GPI equation into four linear terms plus 11 nonlinear terms. The four linear terms are the contributions by the vorticity anomalies, the humidity anomalies, the PI anomalies and the wind shear anomalies. They calculated all terms

and showed that the nonlinear terms are relatively small over eight phases of intraseasonal variability. This is also consistent with that of Camargo et al. (2009) who concluded that "the nonlinearity is weak and thus the effectively linear analysis we have done in this section is valid".

Finally, the results and conclusions in this paper are under the assumption that observational data are reliable. However, some data issues exist in the data sets used in this study. For example, the TC data may have artificial increases in the number (especially for weak TCs such as tropical depressions) due to observational improvements in the recent decades (e.g., Vecchi and Knutson 2008; Landsea et al. 2010; Klotzbach and Landsea 2015). These data issues may affect the correlations and regressions shown in this paper.

Acknowledgments

We thank three reviewers for providing useful comments and suggestions that helped us improve the manuscript. This work was supported by grants from the National Basic Research Program of China (2013CB430301 and 2013CB430304), National Natural Science Foundation (41376015), the National Program on Global Change and Air-Sea Interaction (GASI-IPOVAI-04), and the Pioneer Hundred Talents Program of the Chinese Academy of Sciences. The findings and conclusions in this report are those of the author(s) and do not necessarily represent the views of the funding agency.

References

Balaguru K et al. (2012) Ocean barrier layers' effect on tropical cyclone intensification. Proc Natl Acad Sci 109(36):14343–14347.

Bender MA, Ginis I (2000) Real-case simulations of hurricane–ocean interaction using a high resolution coupled model: effects on hurricane intensity. Mon Weather Rev 128:917–946.

Camargo SJ, Wheeler MC, Sobel AH (2009) Diagnosis of the MJO modulation of tropical cyclogenesis using an empirical index. J Atmos Sci 66:3061–3074.

Carton JA, Giese BS (2008) A reanalysis of ocean climate using simple ocean data assimilation (SODA). Mon Weather Rev 136:2999–3017.

Chen H, Zhang DL, Carton J, Atlas R (2011) On the rapid intensification of Hurricane Wilma (2005). Part I: Model prediction and structural changes. Weather Forecast 26:885–901.

Compo GP et al (2011) The twentieth century reanalysis project. Q J R Meteorol Soc 137:1–28.

Delworth TL, Mann ME (2000) Observed and simulated multidecadal variability in the Northern Hemisphere. Clim Dyn 16:661–676.

Elsberry RL (2014) Advances in research and forecasting of tropical cyclones from 1963 to 2013. Asia-Pac J Atmos 50:3–16.

Elsberry R, Lambert TDB, Boothe MA (2007) Accuracy of Atlantic and eastern North Pacific tropical cyclone intensity forecast guidance. Weather Forecast 22:747–762.

Emanuel K, Nolan DS (2004) Tropical cyclone activity and the global climate system. Proc 26 AMS Conf Hurr Trop Meteor 10:240–241.

Emanuel KA, DesAutels C, Holloway C, Korty R (2004) Environmental control of tropical cyclone intensity. J Atmos Sci 61:843–858.

Enfield DB, Mestas-Nuñez AM, Trimble PJ (2001) The Atlantic multidecadal oscillation and its relation to rainfall and river flows in the continental US. Geophys Res Lett 28:2077–2080.

Enfield DB, Lee SK, Wang C (2006) How are large Western Hemisphere Warm Pools formed? Prog Oceanogr 70(2–4):346–365.

Goldenberg SB, Shapiro LJ (1996) Physical mechanisms for the association of El Nino and West African rainfall with Atlantic major hurricanes. J Climate 9:1169–1187.

Goldenberg SB, Landsea C, Mestas-Nunez AM, Gray WM (2001) The recent increase in Atlantic hurricane activity. Science 293:474–479.

Gray WM (1979) Hurricanes: their formation, structure and likely role in the tropical circulation. In: Shaw DB (ed) Meteorology over the tropical oceans. Royal Meteorological Society, Bracknell, pp 155–218.

Gray WM (1984) Atlantic seasonal hurricane frequency. Part I: El Nino and 30-mb quasi-biennial oscillation influences. Mon Weather Rev 112:1649–1668.

Gray WM (1988) Environmental influences on tropical cyclones. Aust Meteor Mag 36:127–139.

Hendricks EA, Peng MS, Fu B, Li T (2010) Quantifying environmental control on tropical cyclone intensity change. Mon Weather Rev 138:3243–3271.

Hong X et al (2000) The Interaction between Hurricane Opal (1995) and a Warm Core Ring in the Gulf of Mexico. Mon Weather Rev 128:1347–1365.

Hurrel JM (1996) Influence of variations in extratropical wintertime teleconnections on Northern Hemisphere temperature. Geophys Res Lett 23:665–668.

Jiang X, Zhao M, Waliser DE (2012) Modulation of tropical cyclone activity by the tropical intraseasonal oscillation over the Eastern Pacific in a high resolution GCM. J Clim 25:6524–6538.

Kalnay E et al (1996) The NCEP/NCAR 40-year reanalysis project. Bull Am Meteorol Soc 77:437–471.

Kaplan J, DeMaria M (2003) Large-scale characteristics of rapidly intensifying tropical cyclones in the North Atlantic basin. Weather Forecast 18:1093–1108.

Kaplan J, DeMaria M, Knaff JA (2010) A revised tropical cyclone rapid intensification index for the Atlantic and East Pacific basins. Weather Forecast 25:220–241.

Kaplan J et al (2015) Evaluating environmental impacts on tropical cyclone rapid intensification predictability utilizing statistical models. Weather Forecast 30:1374–1396.

Klotzbach PJ (2012) El Nino-Southern Oscillation, the Madden-Julian Oscillation and Atlantic basin tropical cyclone rapid intensification. J Geophys Res 117:D14104.

Klotzbach PJ, Landsea CW (2015) Extremely intense hurricanes: Revisiting Webster et al. (2005) after 10 years. J Clim 28:7621–7629.

Landsea CW, Vecchi GA, Bengtsson L, Knutson TR (2010) Impact of duration thresholds on Atlantic tropical cyclone counts. J Clim 23:2508–2519.

Lee CY, Tippett MK, Sobel AH, Camargo SJ (2016) Rapid intensification and the bimodal distribution of tropical cyclone intensity. Nat Commun. 7:10625.

Leipper D (1967) Observed ocean conditions and Hurricane Hilda, 1964. J Atmos Sci 24:182–196.

Leipper D, Volgenau D (1972) Hurricane heat potential of the Gulf of Mexico. J Phys Oceanogr 2:218–224.

Lin II, Wu CC, Emanuel K, Lee IH, Wu CR, Pun IF (2005) The interaction of Supertyphoon Maemi (2003) with a warm ocean eddy. Mon Weather Rev 133(9):2635–2649.

Lin II, Wu CC, Pun IF, Ko DS (2008) Upper-ocean thermal structure and the western North Pacific category 5 typhoons. Part I: ocean features and the category 5 typhoons' intensification. Mon Weather Rev 136(9):3288–3306.

Lin II, Chen CH, Pun IF, Liu WT, Wu CC (2009a) Warm ocean anomaly, air sea fluxes, and the rapid intensification of tropical cyclone Nargis (2008). Geophys Res Lett 36:L03817.

Lin II, Pun IF, Wu CC (2009b) Upper ocean thermal structure and the western North Pacific category-5 typhoons part II: dependence on translation speed. Mon Weather Rev 137(11):3744–3757.

Medhaug I, Furevik T (2011) North Atlantic 20th century multidecadal variability in coupled climate models: sea surface temperature and ocean overturning circulation. Ocean Sci 7:389–404.

Merrill RT (1988) Environmental influences on hurricane intensification. J Atmos Sci 45:1678–1687.

Quenouille MH (1952) Associated measurements. Butterworths Scientific, London, p 242.

Rappaport EN et al (2009) Advances and challenges at the National Hurricane Center. Weather Forecast 24:395–419.

Shay LK, Goni GJ, Black PG (2000) Effects of a warm oceanic feature on Hurricane. Opal. Mon Weather Rev 128:1366–1383.

Shieh OH, Colucci SJ (2010) Local minimum of tropical cyclogenesis in the eastern Caribbean. Bull Am Meteor Soc 91:185–196.

Shu SJ, Ming J, Chi P (2012) Large-scale characteristics and probability of rapidly intensifying tropical cyclones in the western north pacific basin. Weather Forecast 27:411–423.

Smith TM, Reynolds RW, Peterson TC, Lawrimore J (2008) Improvements to NOAA's historical merged land–ocean surface temperature analysis (1880–2006). J Clim 21:2283–2296.

Sutyrin GG, Khain AP (1984) Effect of the ocean–atmosphere interaction on the intensity of a moving tropical cyclone. Atmos Ocean Phys 20:697–703.

Vecchi GA, Knutson TR (2008) On estimates of historical North Atlantic tropical cyclone activity. J Clim 21:3580–3600.

Vecchi GA, Soden BJ (2007) Increased tropical Atlantic wind shear in model projections of global warming. Geophys Res Lett 34:L08702.

Vimont DJ, Battisti DS, Hirst AC (2001) Footprinting: a seasonal connection between the tropics and mid-latitudes. Geophys Res Lett 28:3923–3926.

Vimont DJ, Battisti DS, Hirst AC (2003) The seasonal footprinting mechanism in the CSIRO general circulation models. J Clim 16:2653–2667.

Wang C (2007) Variability of the Caribbean low-level jet and its relations to climate. Clim Dyn 29:411–422.

Wang C, Enfield DB (2001) The tropical western hemisphere warm pool. Geophys Res Lett 28:1635–1638.

Wang C, Enfield DB (2003) A further study of the tropical Western Hemisphere warm pool. J Clim 16:1476–1493.

Wang C, Enfield DB, Lee SK, Landsea CW (2006) Influences of the Atlantic warm pool on Western Hemisphere summer rainfall and Atlantic hurricanes. J Clim 19:3011–3028.

Wang C, Lee SK, Enfield DB (2008) Atlantic warm pool acting as a link between Atlantic multidecadal oscillation and Atlantic tropical cyclone activity. Geochem Geophys Geosyst 9:Q05V03.

Wang C, Dong S, Evan AT, Foltz GR, Lee SK (2012) Multidecadal covariability of North Atlantic sea surface temperature, African dust, Sahel rainfall and Atlantic hurricanes. J Clim 25:5404–5415.

Xie SP (1999) A dynamic ocean-atmosphere model of the tropical Atlantic decadal variability. J Clim 12:64–70.

Xie SP, Philander SGH (1994) A coupled ocean–atmosphere model of relevance to the ITCZ in the eastern Pacific. Tellus 46A:340–350.

Zhang L, Wang C (2012) Remote influences on freshwater flux variability in the Atlantic warm pool region. Geophys Res Lett 39:L19714.

Table 1. Correlations of RI, TC, TS, H and MH with total climate indices.

	ENSO	AMO	NAO	NAO (JFM)	MDR SST	AWP
RI	−0.45**	0.22	−0.02	−0.39**	0.32*	0.39**
TC	−0.22	−0.10	0.23	0.06	−0.03	0.03
TS	−0.26	0.46**	−0.11	0.04	0.42**	0.44**
H	−0.35**	0.49**	−0.13	−0.17	0.53**	0.52**
MH	−0.31*	0.52**	−0.07	−0.28*	0.55**	0.49**

All climate indices are calculated during the Atlantic hurricane season of June–November (JJASON), except for the NAO whose winter (January–March, JFM) index is also included.

"*" and "**" indicate the correlations are above the 95 and 99% significance levels, respectively.

Table 2. Correlations of RI, TC, TS, H and MH with climate indices on interannual time scales.

	ENSO	AMO	NAO	NAO (JFM)	MDR SST	AWP
RI	−0.48**	0.16	0.19	−0.25	0.22	0.25
TC	−0.35*	0.15	0.33*	0.03	0.21	0.25
TS	−0.44**	0.18	0.11	−0.08	0.31	0.31*
H	−0.48**	0.35*	0.04	−0.22	0.41**	0.41**
MH	−0.43**	0.22	0.18	−0.30	0.34*	0.25

All climate indices are calculated during the Atlantic hurricane season of June–November (JJASON), except for the NAO whose winter (January–March, JFM) index is also included.

"*" and "**" indicate the correlations are above the 95 and 99% significance levels, respectively.

Table 3. Correlations of RI, TC, TS, H and MH with climate indices on multidecadal time scales.

	ENSO	AMO	NAO	NAO (JFM)	MDR SST	AWP
RI	−0.31	0.39	−0.51*	−0.61*	0.51*	0.69**
TC	−0.02	−0.26	0.14	0.11	−0.31	−0.17
TS	0.22	0.71**	−0.65**	0.21	0.55*	0.57*
H	0.21	0.81**	−0.72**	−0.03	0.73**	0.74**
MH	0.06	0.91**	−0.73**	−0.25	0.87**	0.86**

All climate indices are calculated during the Atlantic hurricane season of June–November (JJASON), except for the NAO whose winter (January–March, JFM) index is also included.

"*" and "**" indicate the correlations are above the 95 and 99% significance levels, respectively.

Table 4. Correlations of RI with the numbers of TC, TS, H and MH.

	TC	TS	H	MH
RI (total)	0.41**	0.59**	0.61**	0.63**
RI (interannual)	0.61**	0.71**	0.68**	0.71**
RI (multidecadal)	0.18	0.45*	0.58*	0.59*

The correlations are calculated based on the total indices and the indices on interannual and multidecadal time scales.

"*" and "**" indicate the correlations are above the 95 and 99% significance levels, respectively.

Table 5. Correlations of TCHP, VWS and RHUM with the numbers of RI, TC, TS, H and MH.

	TCHP	VWS	RHUM
RI	0.32*	−0.53**	0.31*
TC	0.01	−0.08	0.13
TS	0.40**	−0.51**	0.37**
H	0.49**	−0.57**	0.49**
MH	0.44**	−0.65**	0.51**

The correlations are calculated based on the total TCHP, VWS and RHUM time series during JJASON in the MDR region (10°N–20°N, 85°W–15°W).

"*" and "**" indicate the correlations are above the 95% and 99% significance levels, respectively.

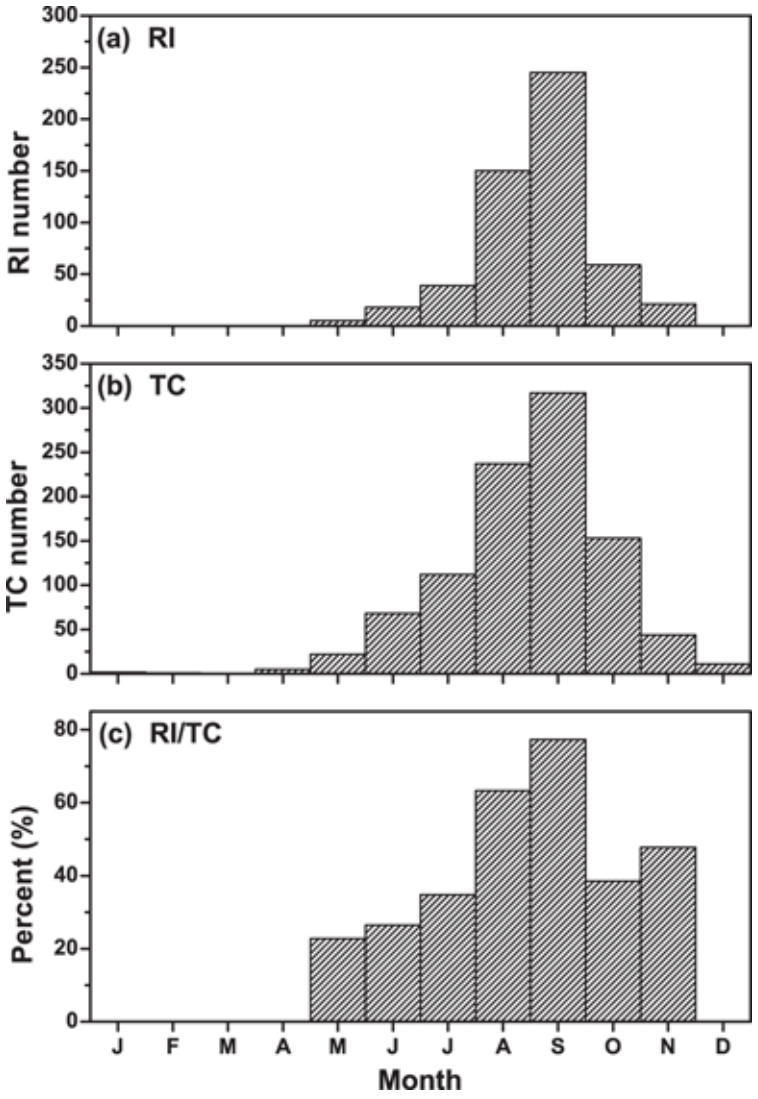

Fig. 1. Seasonal distributions of (a) the number of RI events, (b) the number of TCs, and (c) the percentage of TCs undergoing RI in the North Atlantic from 1950– 2014.

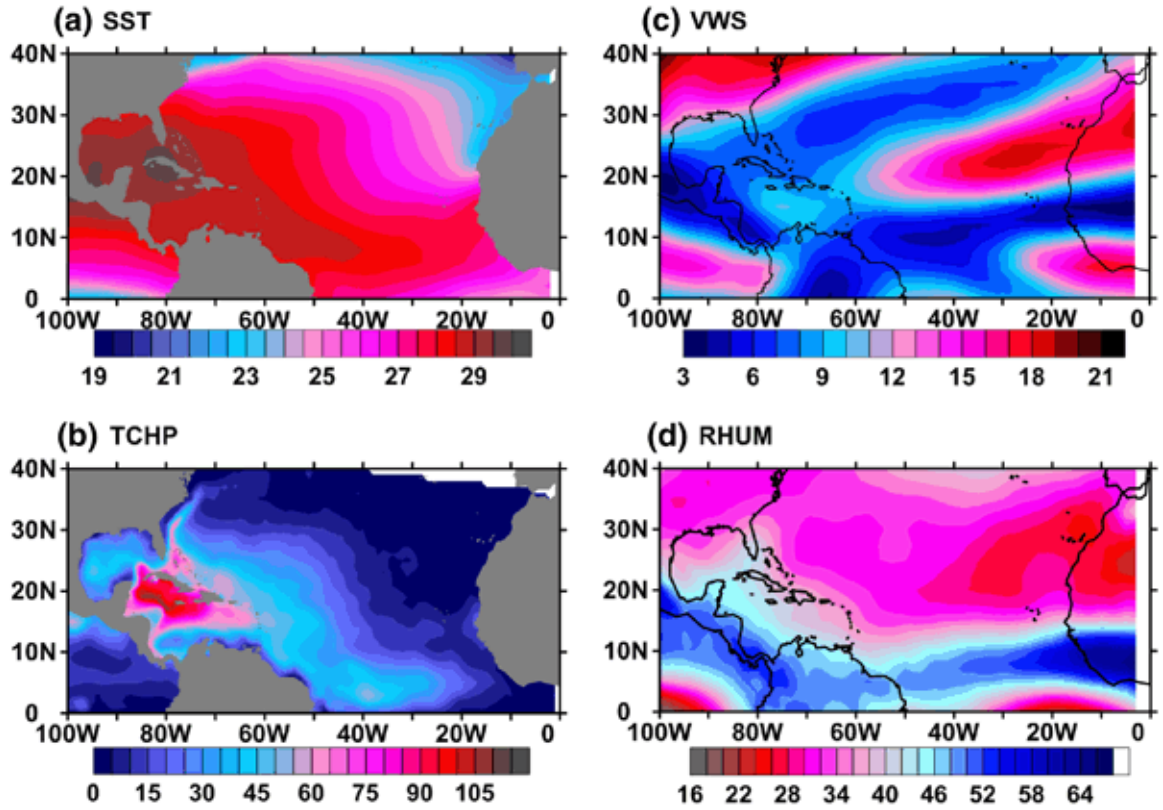

Fig. 2. Monthly climatology of (a) SST (°C), (b) TCHP (kJ/cm^2), (c) VWS (m/s), and (d) RHUM (%) in September.

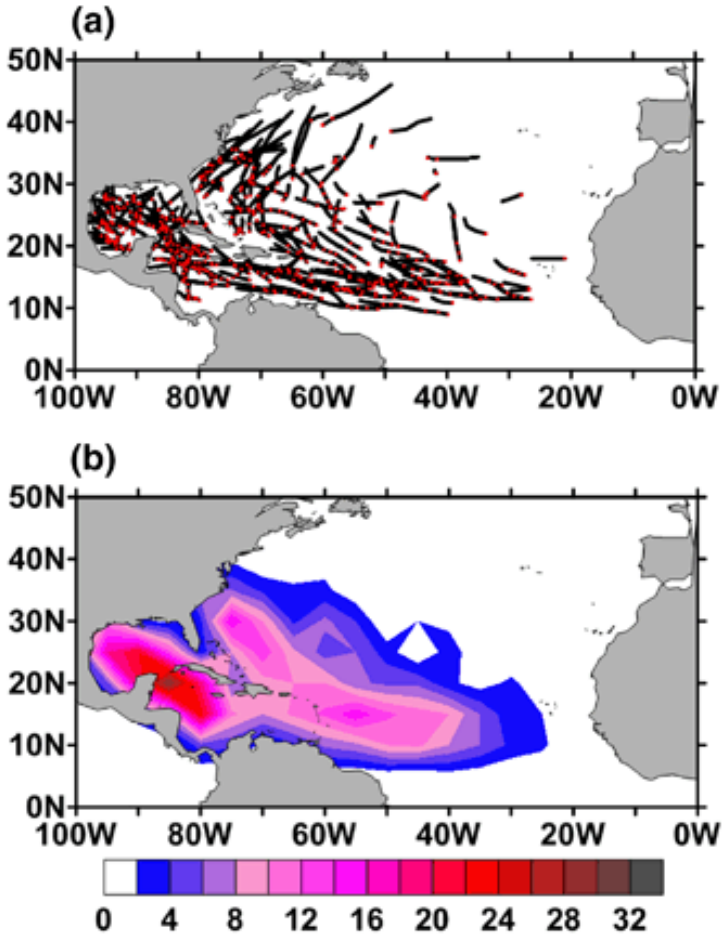

Fig. 3. (a) 24-hour tracks of RI events. The *red dots* represent the initial location of RI events. (b) RI number in each 5° × 5° *box* during 1950–2014.

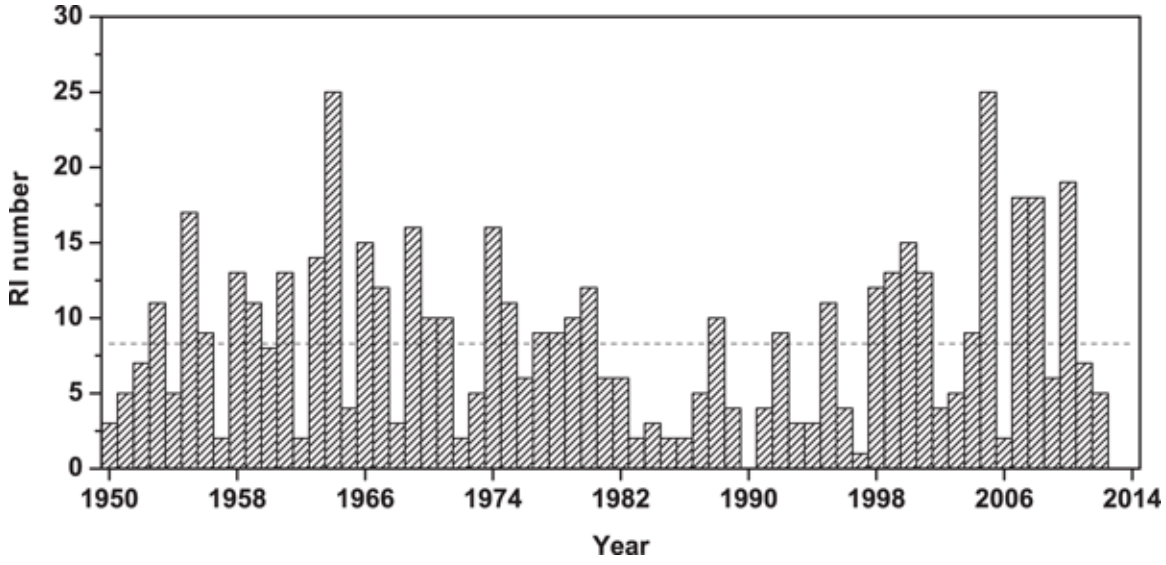

Fig. 4. Time series of the annual RI number during 1950–2014. The *dashed line* represents the mean RI value.

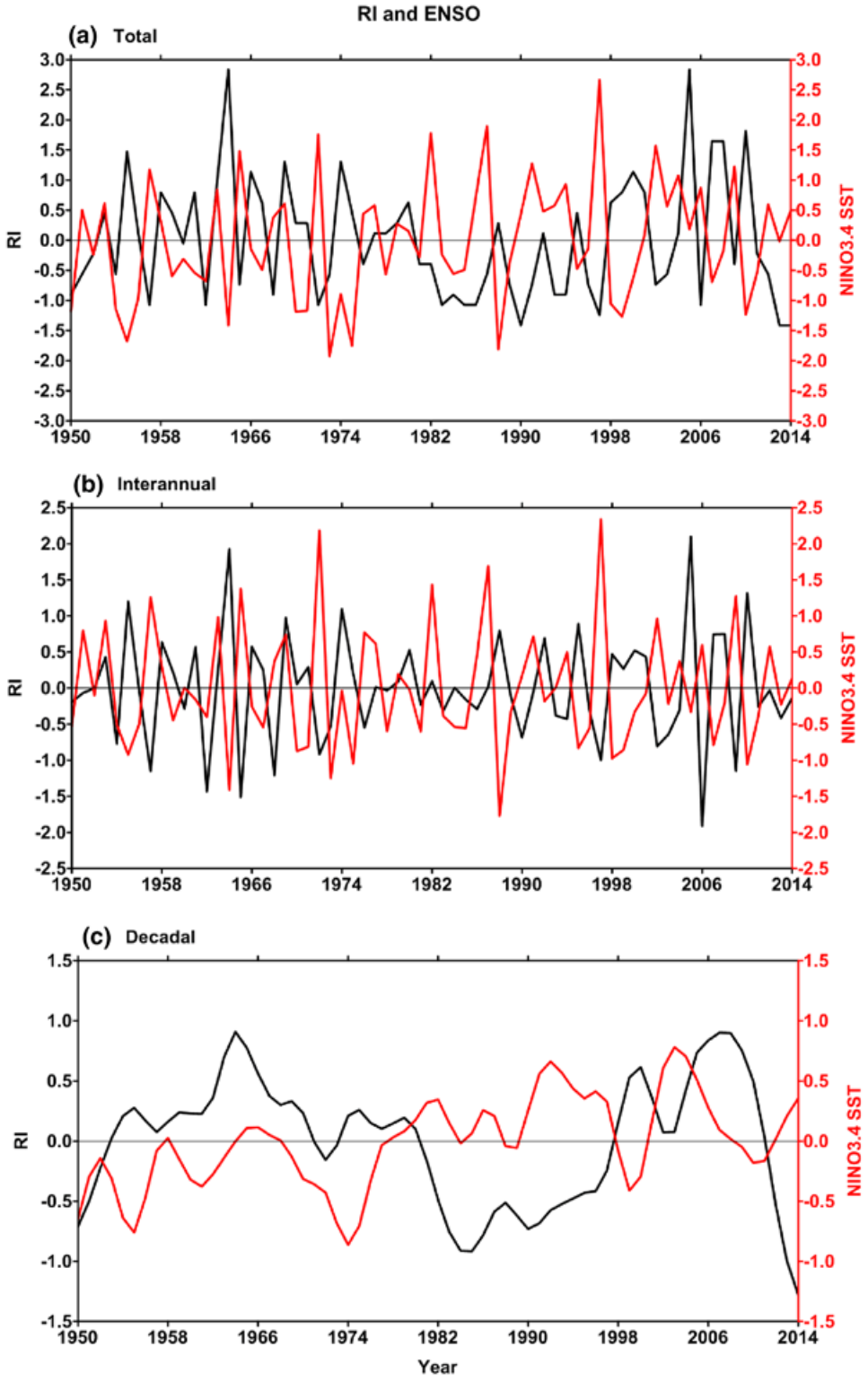

Fig. 5. Time series of annual RI number (*black curve*) and JJASON NINO3.4 index (*red curve*) for (a) total, (b) interannual, and (c) multidecadal variations. The RI time series is standardized by the mean and standard deviation of the annual RI number during 1950–2014.

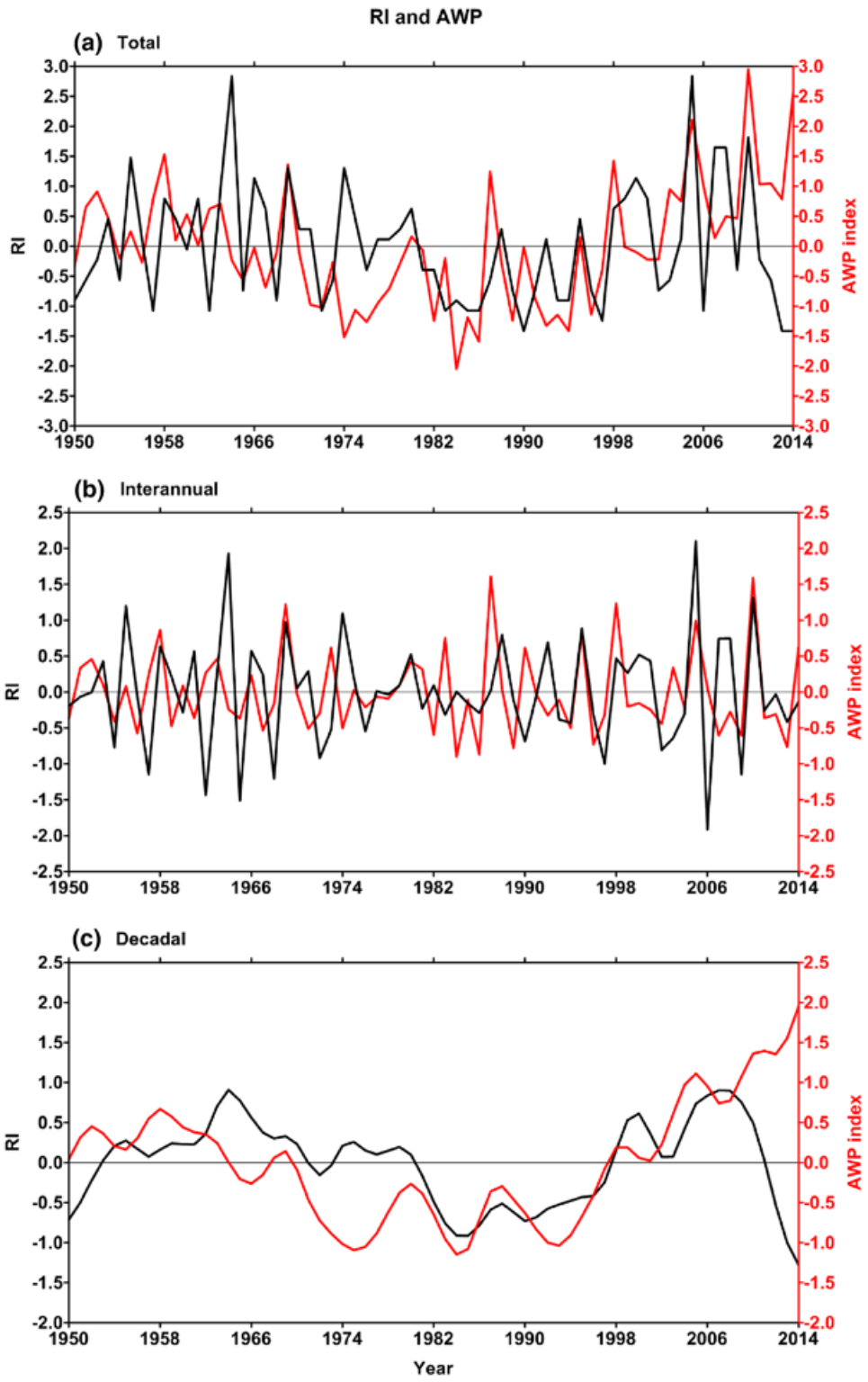

Fig. 6. Time series of annual RI number (*black curve*) and JJASON AWP index (*red curve*) for (a) total, (b) interannual, and (c) multidecadal variations. The RI time series is standardized by the mean and standard deviation of the annual RI number during 1950–2014.

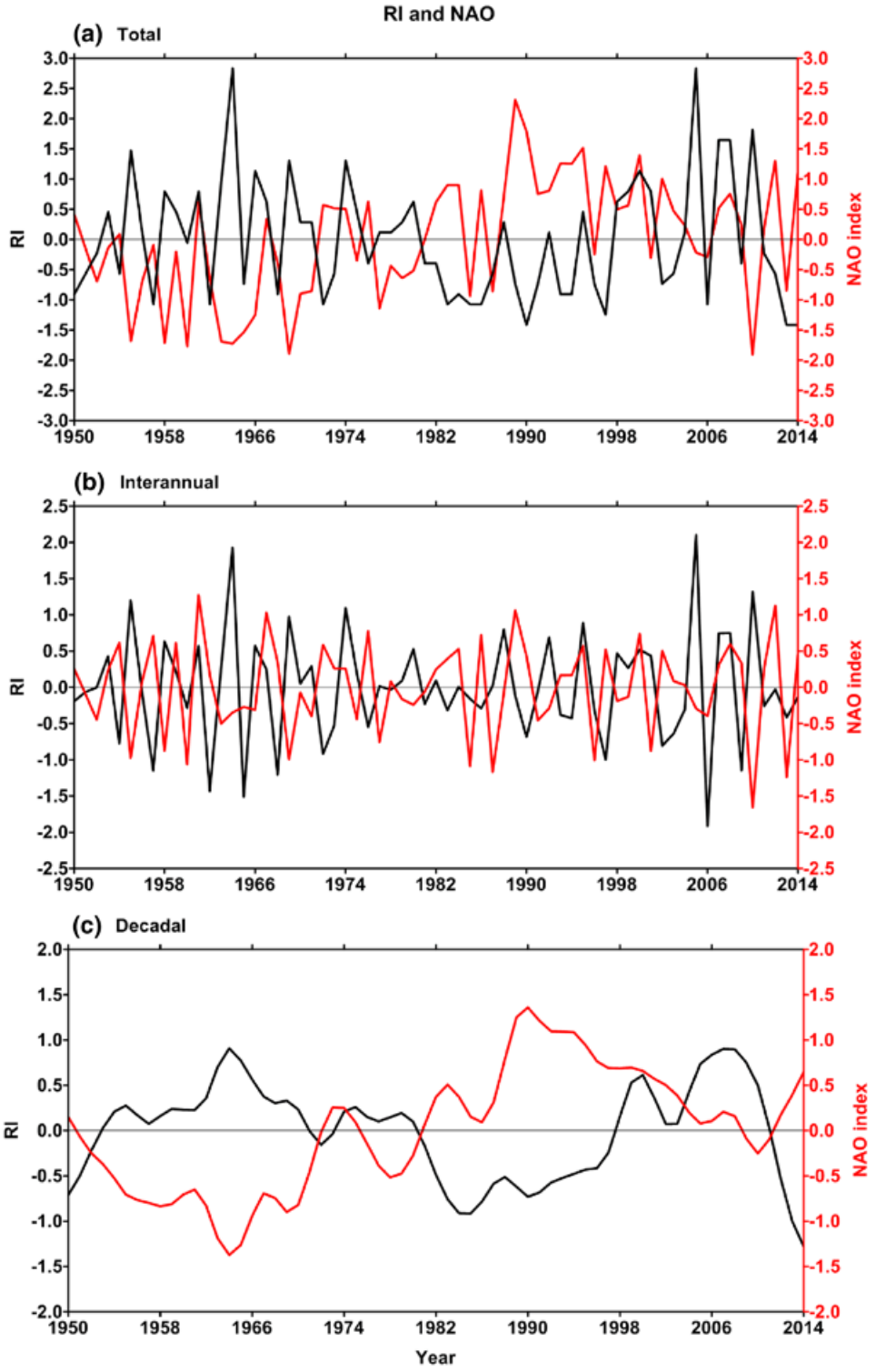

Fig. 7. Time series of annual RI number (*black curve*) and JFM NAO index (*red curve*) for (a) total, (b) interannual, and (c) multidecadal variations. The RI time series is standardized by the mean and standard deviation of the annual RI number during 1950–2014.

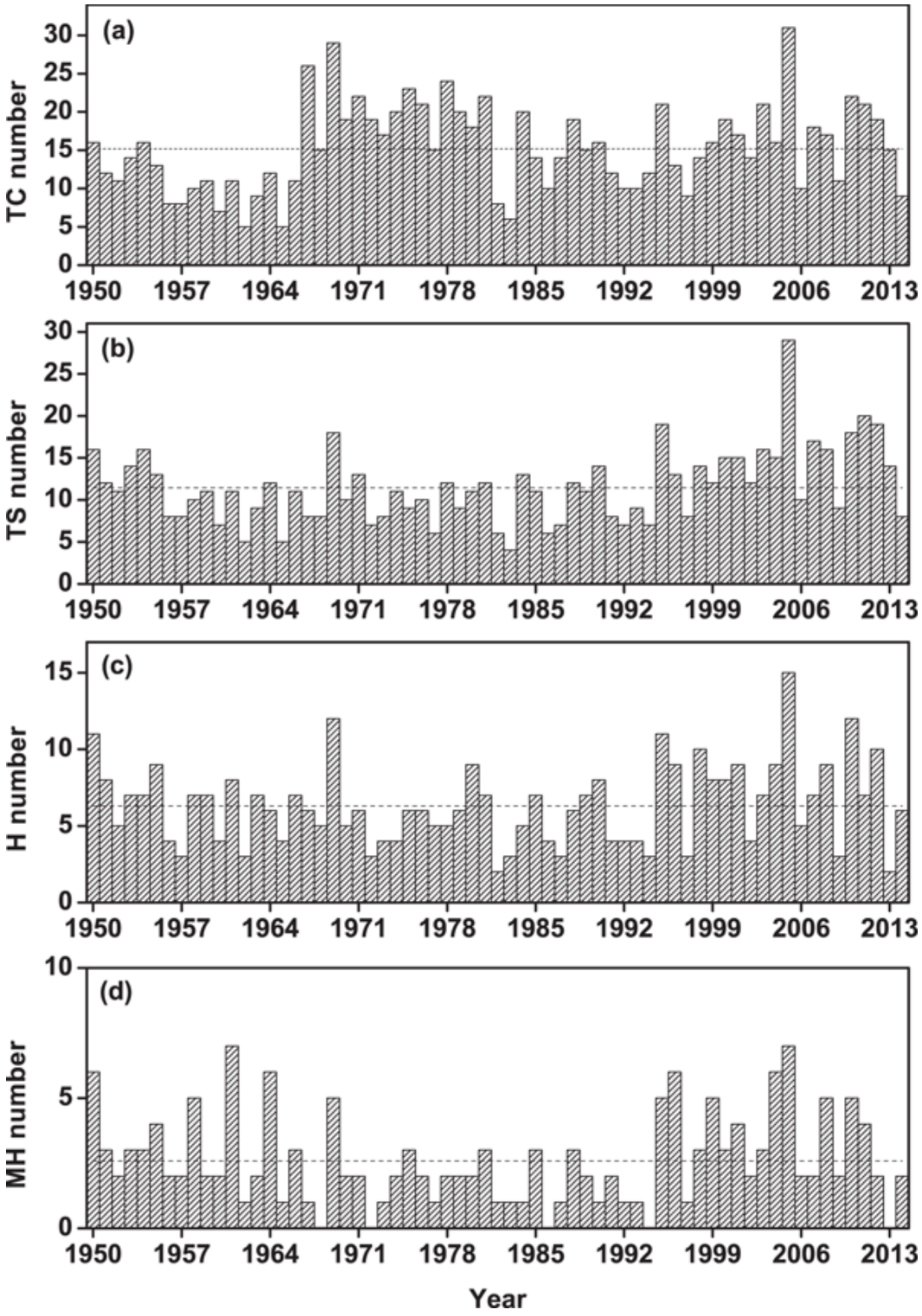

Fig. 8. Time series of the annual numbers of (a) TCs, (b) tropical storms (TS), (c) hurricanes (H), and (d) major hurricanes (MH) during 1950–2014. The *dashed lines* represent the corresponding mean RI values.

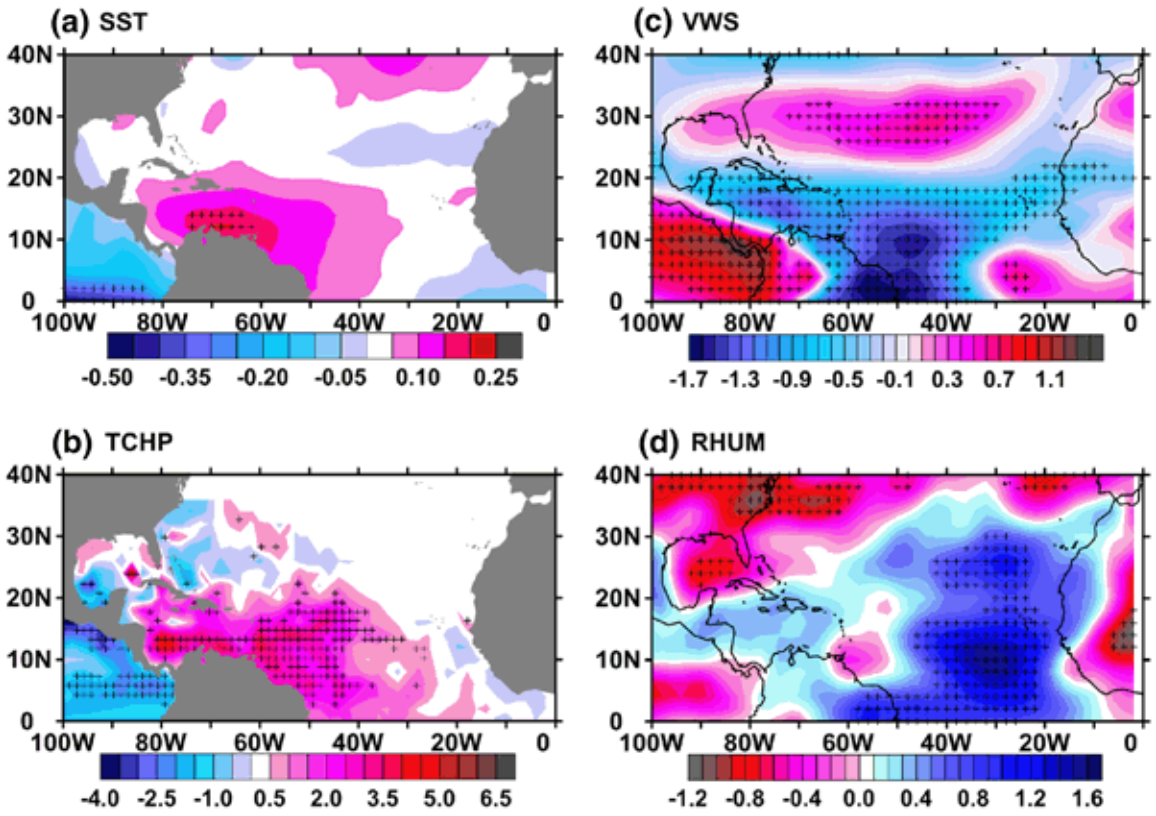

Fig. 9. Regressions of standardized annual RI number onto the (a) SST, (b) TCHP, (c) VWS, and (d) RHUM during JJASON. The SST, TCHP, VWS and RHUM for months of JJASON are linearly detrended prior to the analysis. The cross sign indicates the regions where the regression exceeds the 95% significance level.

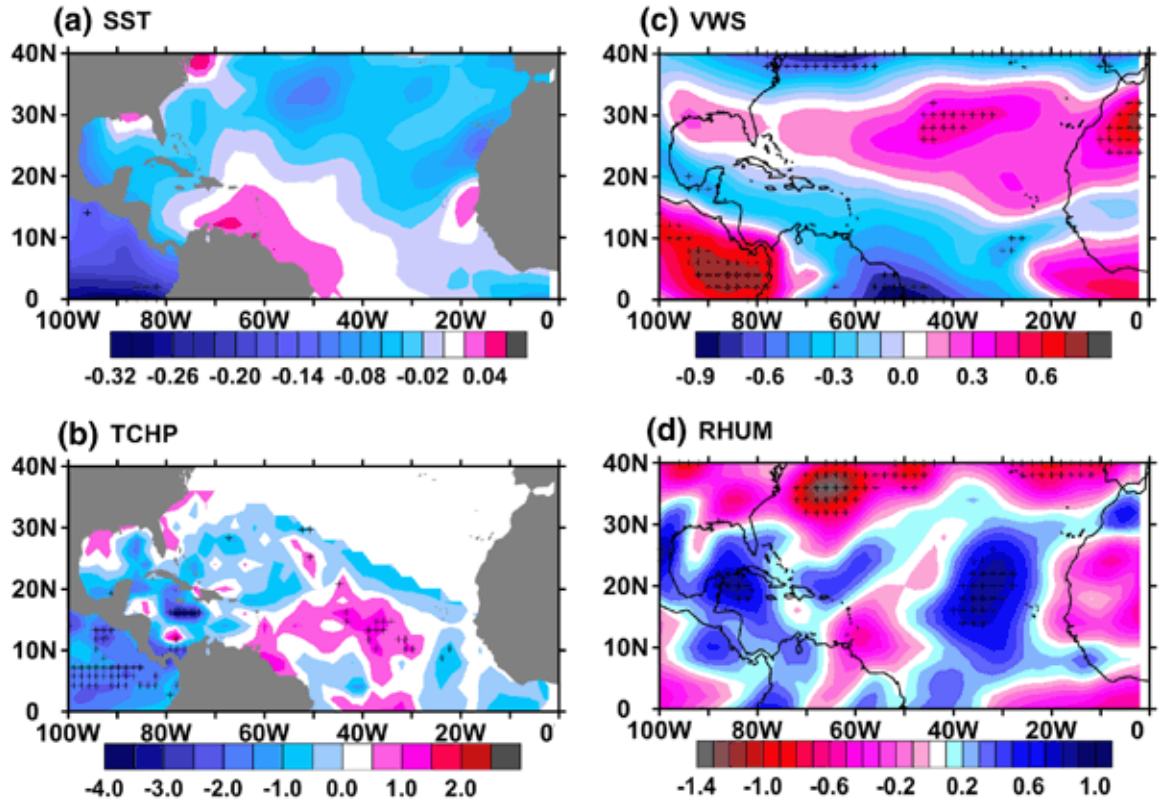

Fig. 10. Regressions of TC number onto the (a) SST, (b) TCHP, (c) VWS, and (d) RHUM during JJASON. The SST, TCHP, VWS and RHUM for months of JJASON are linearly detrended prior to the analysis. The *cross sign* indicates the regions where the regression exceeds the 95% significance level.

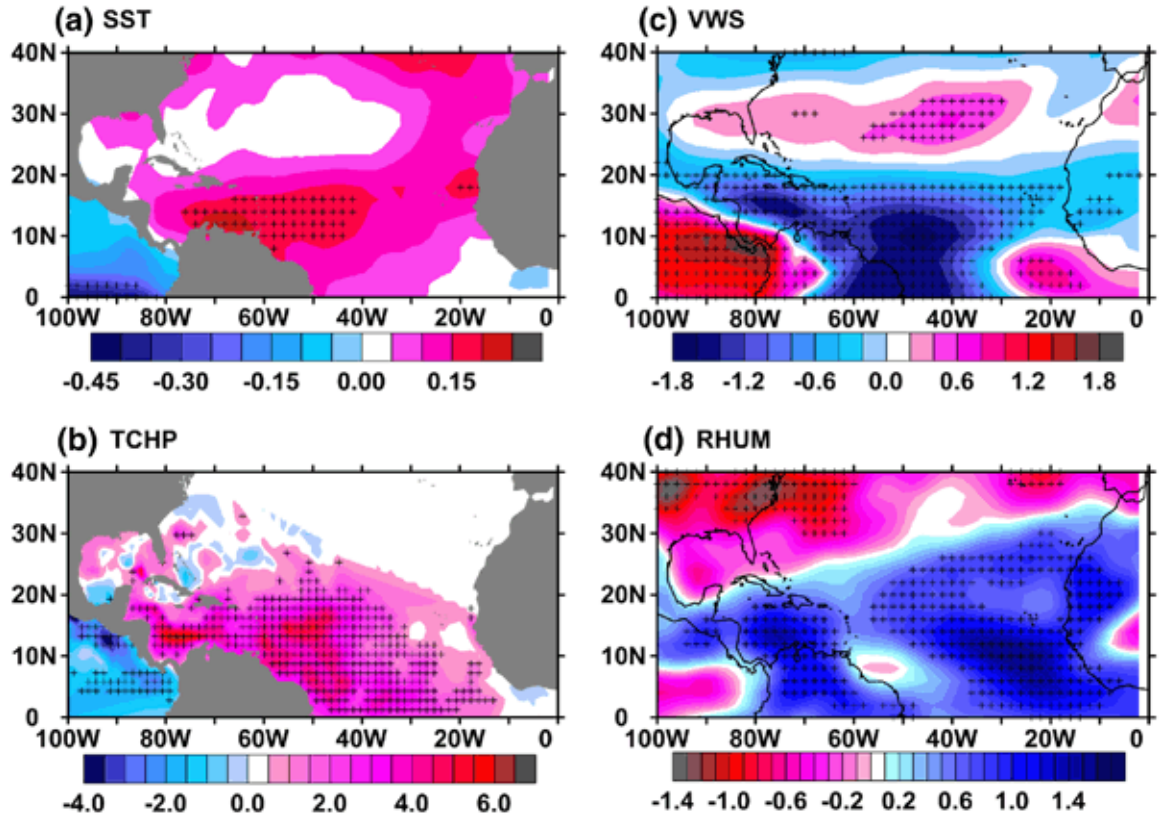

Fig. 11. Regressions of H (Hurricane) number onto the (a) SST, (b) TCHP, (c) VWS and (d) RHUM during JJASON. The SST, TCHP, VWS and RHUM for months of JJASON are linearly detrended prior to the analysis. The *cross sign* indicates the regions where the regression exceeds the 95% significance level.

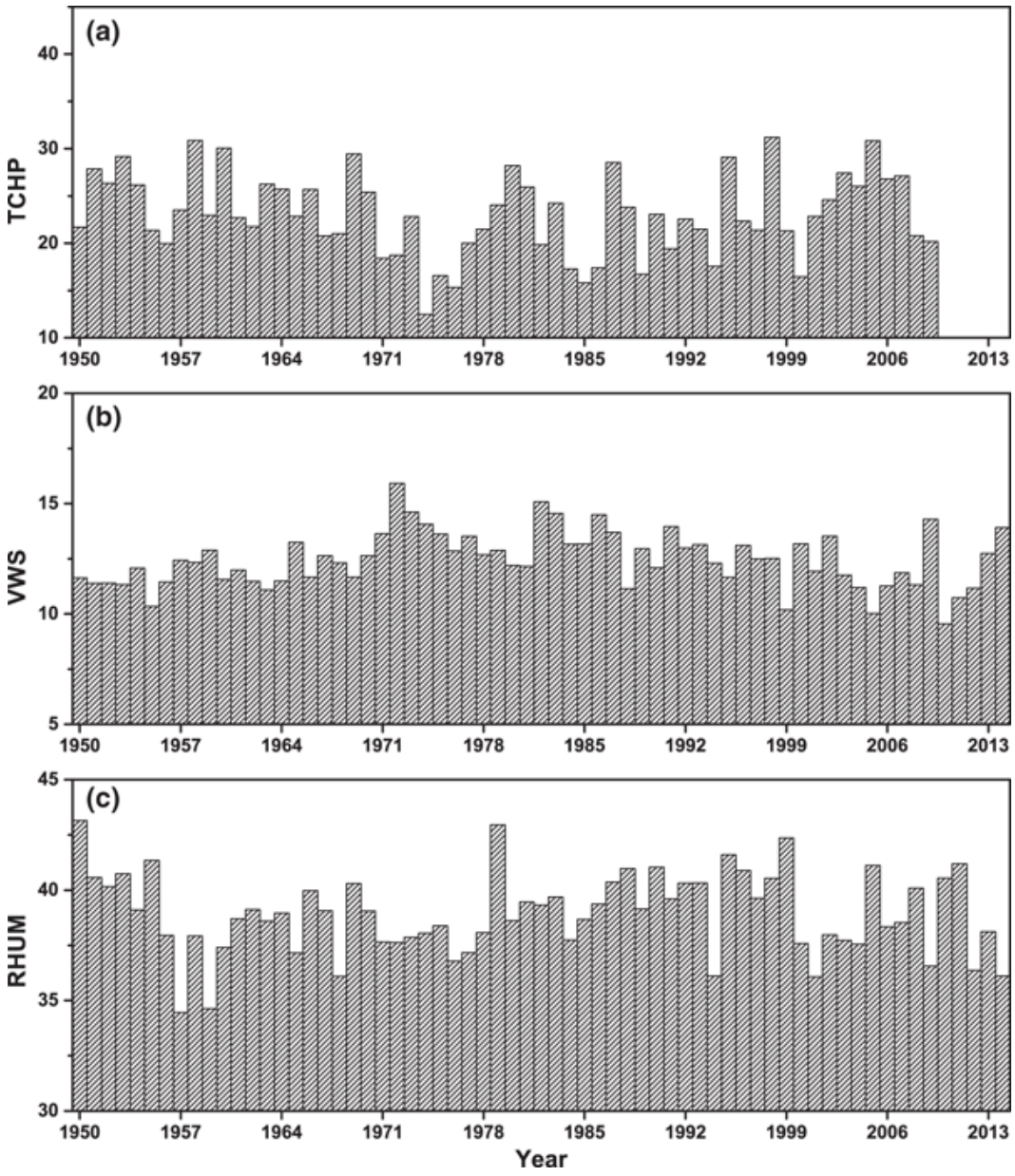

Fig. 12. Time series of (a) TCHP (kJ/cm^2), (b) VWS (m/s) and (c) RHUM (%) in the main development region (MDR) during June–November. The MDR is defined in the region of 10°N–20°N, 85°W–15°W. TCHP, VWS and RHUM are linearly detrended. The time series of TCHP is to 2010 because of SODA availability.

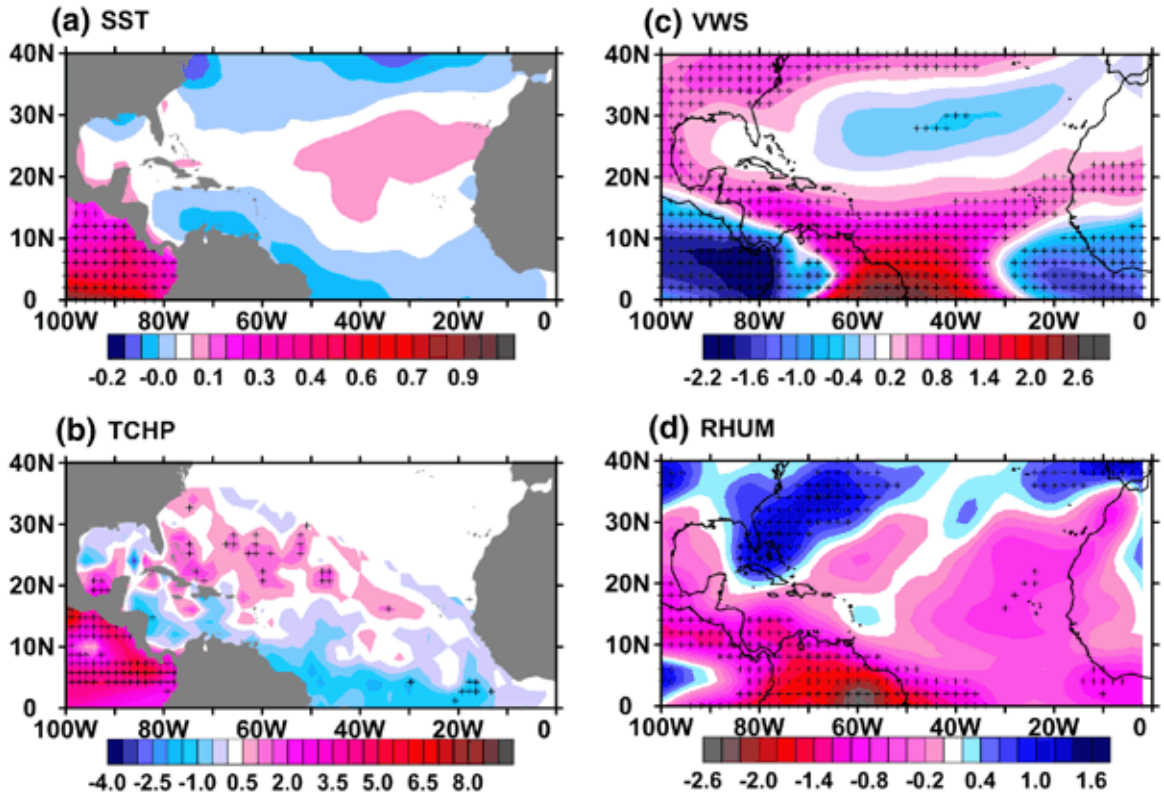

Fig. 13. Regressions of the JJASON NINO3.4 SST index onto (a) SST, (b) TCHP, (c) VWS and (d) RHUM during JJASON. The SST, TCHP, VWS and RHUM for months of JJASON are linearly detrended prior to the analysis. The *cross sign* indicates the regions where the regression exceeds the 95% significance level.

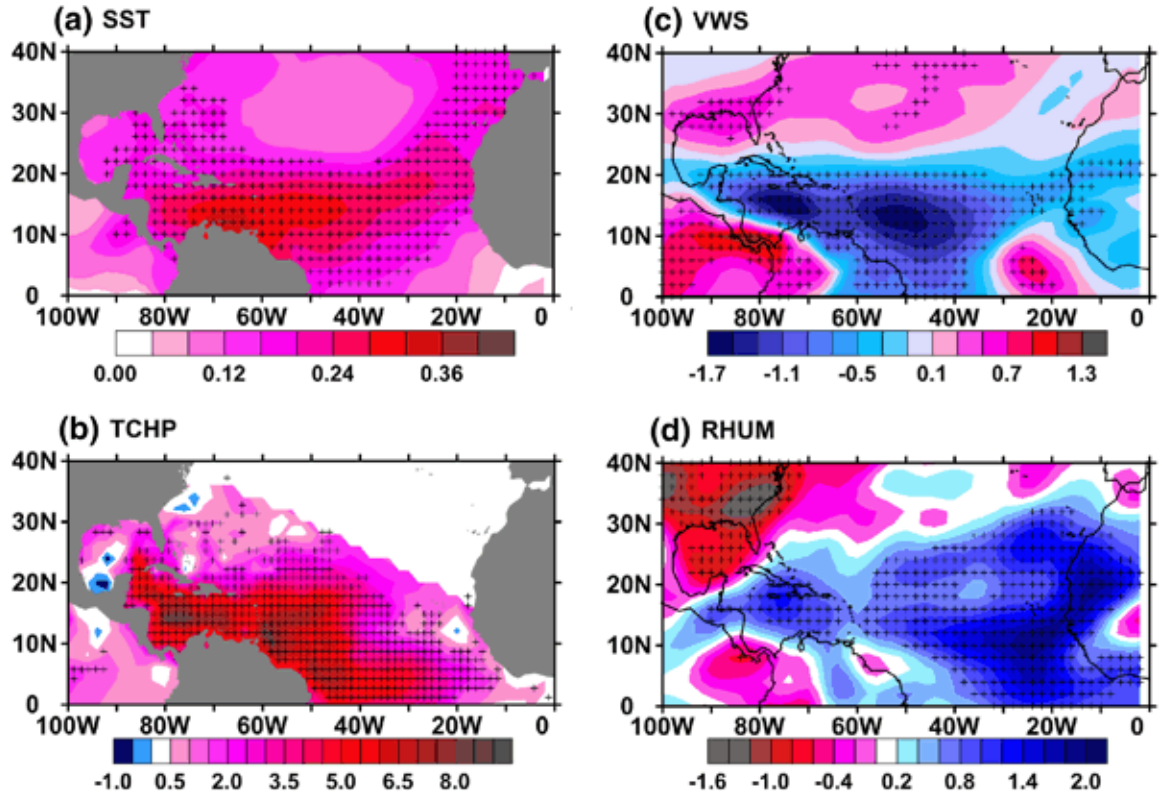

Fig. 14. Regressions of the JJASON AWP index onto (a) SST, (b) TCHP, (c) VWS, and (d) RHUM during JJASON. The SST, TCHP, VWS and RHUM for months of JJASON are linearly detrended prior to the analysis. The *cross sign* indicates the regions where the regression exceeds the 95% significance level.

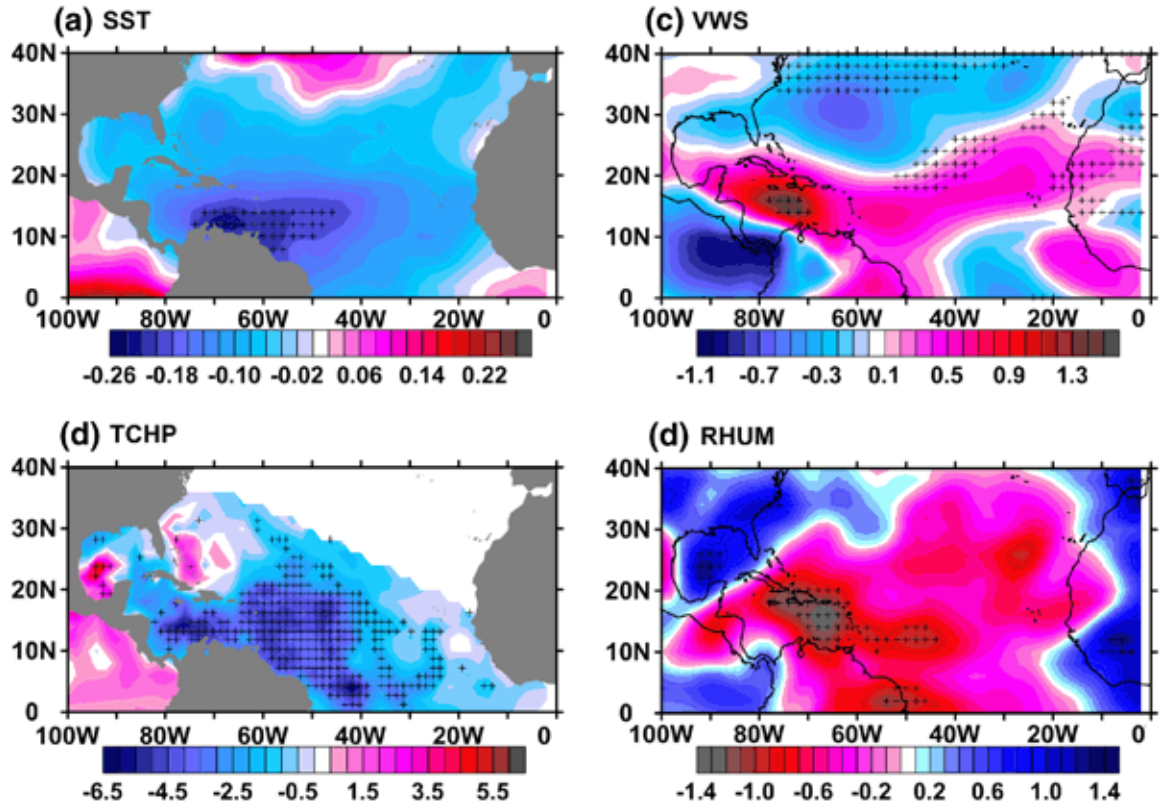

Fig. 15. Regressions of the JFM NAO index onto (a) SST, (b) TCHP, (c) VWS and (d) RHUM during JJASON. The SST, TCHP, VWS and RHUM for months of JJASON are linearly detrended prior to the analysis. The *cross sign* indicates the regions where the regression exceeds the 95% significance level.